High power impulse magnetron sputtering: Current-voltage-time characteristics indicate the onset of sustained self-sputtering

André Anders[a] and Joakim Andersson
Lawrence Berkeley National Laboratory, University of California, 1 Cyclotron Road, Berkeley, California 94720, USA

Arutiun Ehiasarian
Materials and Engineering Research Institute, Sheffield Hallam University, Howard St., Sheffield S1 1WB, United Kingdom

(Received 3 August 2007; accepted 1 October 2007; published online 4 December 2007)

The commonly used current-voltage characteristics are found inadequate for describing the pulsed nature of the high power impulse magnetron sputtering (HIPIMS) discharge; rather, the description needs to be expanded to current-voltage-time characteristics for each initial gas pressure. Using different target materials (Cu, Ti, Nb, C, W, Al, and Cr) and a pulsed constant-voltage supply, it is shown that the HIPIMS discharges typically exhibit an initial pressure dependent current peak followed by a second phase that is power and material dependent. This suggests that the initial phase of a HIPIMS discharge pulse is dominated by gas ions, whereas the later phase has a strong contribution from self-sputtering. For some materials, the discharge switches into a mode of sustained self-sputtering. The very large differences between materials cannot be ascribed to the different sputter yields but they indicate that generation and trapping of secondary electrons play a major role for current-voltage-time characteristics. In particular, it is argued that the sustained self-sputtering phase is associated with the generation of multiply charged ions because only they can cause potential emission of secondary electrons, whereas the yield caused by singly charged metal ions is negligibly small. © *2007 American Institute of Physics*. [DOI: 10.1063/1.2817812]

I. INTRODUCTION

High power impulse magnetron sputtering (HIPIMS) is an emerging physical vapor deposition (PVD) technology. It is characterized by a high pulse power density at the sputtering target, which is typically two orders of magnitude greater than the average power density. We adopt the term HIPIMS, as opposed to high power pulse magnetron sputtering, because the latter is inconsistently used for either HIPIMS-like systems or for medium frequency pulsed sputtering with very large area targets. In the latter case, even as the power is high, the pulse power *density* does not much exceed the average power density.

With greatly enhanced power density, ionization of sputtered atoms can occur to a much larger extent. The presence of ionized sputtered material is of great importance to some PVD applications such as the filling of trenches and vias of semiconductor microprocessors. Additionally, HIPIMS may be used for applications that are traditionally served by cathodic arc plasma processing such as substrate etching[1] and film deposition.[2] Ionization of the sputtered material enables the processes of self-ion-assisted deposition and energetic condensation.[3–5]

The roots of ionized sputtering may be traced back to research in Japan some 30 years ago when Hosokawa *et al.* noticed a discrepancy between the measured and calculated copper and aluminum deposition rates.[6] They estimated that in the case of aluminum, about 18% of the ion current to the target are due to ionized sputtered atoms, which cause self-sputtering. A few years later, they published a condition for sustained self-sputtering, i.e., a condition for sputtering that exclusively relies on self-sputtering. Argon, or a similar gas, is only needed to get the process started and may well be shut off afterward.[7] The sustained sputter process can operate with ionized metal only when the power density is very high[8] (typically several 100 $\mathrm{W/cm^2}$). The condition for sustained self-sputtering reads

$$\alpha\beta\gamma_{SS} \geqslant 1, \tag{1}$$

where α is the ionization probability, β is the probability that a sputtered and ionized atom will return to the target, and γ_{SS} is the self-sputter yield. Since $\alpha<1$ and $\beta<1$, the condition $\gamma_{SS}>1$ is necessary but not sufficient for sustained self-sputtering.

Sustained self-sputtering has been demonstrated by several researchers but only for a very limited number of materials. For example, Posadowski and Radsimski[9] showed that the principle works for copper and silver, which are metals of very high self-sputter yield. The experiments showed that sustaining the self-sputtering without processing gas required operation with a high current density on the target. This suggested to go to even higher current density (or, equivalently, power density), which is only possible by using pulses in order to not exceed the average power rating of the magnetron.

At a 1996 symposium in Berkeley, Bugaev *et al.*[10] reported about pulsing a filament-assisted, hollow cathode magnetron to high power, with a pulse voltage up to 800 V

[a]Author to whom correspondence should be addressed. Electronic mail: aanders@lbl.gov

and a peak current of 450 A, leading to a deposition rate of 11 μm/min for copper. In 1999, Kouznetsov *et al.*[11] published their much-cited work in which they explicitly outline the possibility to operate a *planar* magnetron at very high power density, with peak power soon to approach the 1 MW level, leading to deposition of the target material from the plasma phase, as opposed to from the neutral vapor phase of sputtered atoms. Although the number of papers in the field of HIPIMS has grown since then, many aspects of the complicated physics have not been fully understood.

In the following, we report on experiments using a constant voltage HIPIMS power supply and focus on measuring and interpreting the current-voltage characteristics for a number of different target materials. We will show that the current-voltage characteristic cannot be reduced to a single curve representing current-voltage pairs for given conditions (pressure, geometry, etc.) but rather one needs to map the current-voltage-time space for each of those conditions. This can be accomplished by providing a set of time-dependent current curves, each taken at a fixed voltage.

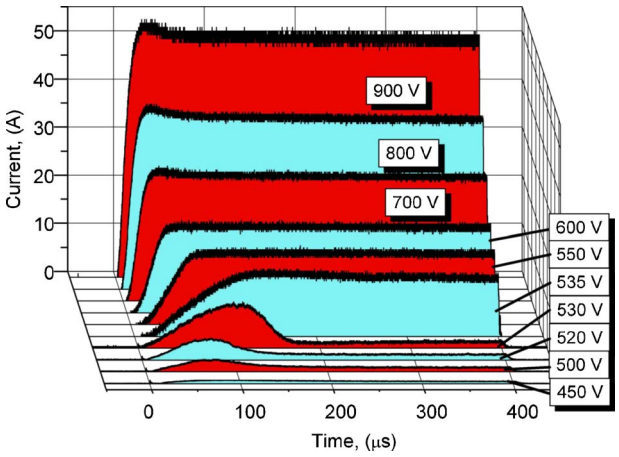

FIG. 1. (Color online) Current pulse shapes at different constant voltage for a copper magnetron discharge (2 in. target) in argon at 1.8 Pa. The actual target voltage is constant and equal to the nominal voltage up to about 800 V; the target voltage starts to slightly droop for higher voltages, indicating the limited stored energy of the power supply. As the voltage approaches the supply's limit of 1000 V, the actual voltage droops and shows less stability. For the highest setting, a shorter pulse of only 300 μs was used.

II. EXPERIMENTAL

The experiments were carried out using a 2 in. (5 cm) planar, balanced magnetron. The targets were $\frac{1}{4}$ in. (6.25 mm) thick; the magnetic field induction at the center of the target surface was 64 mT and lower elsewhere; the diameter of the circular racetrack was 25 mm. We intentionally used such a small magnetron because it allowed us to achieve very high power density. The peak power density was up to 5 kW/cm^2 averaged over the whole target area, and even exceeded 10 kW/cm^2 when considering the more physically relevant, effective racetrack area of about 10 cm^2 or less.

The power was supplied by a slightly modified SPIK2000A pulse power supply (Melec GmbH) operating in the unipolar negative mode at constant voltage. A great feature of this pulser is the ability to freely select the pulse length. The short pulse limit is given by the pulser to 5 μs, and the long pulse limit by the capacitively stored energy, which practically means several milliseconds (one would see a large voltage droop, especially at high current). We are especially interested in pulses longer than 100 μs because this allows the discharge to evolve into the metal discharge phase, as we will discuss. However, the allowable average power to the magnetron of 1 kW, determined by cooling, was a limiting factor that needed to be taken into account. Hence, long pulse operation necessarily implied to have long pauses between pulses (typically 20 ms). The nominal voltage of the pulser was adjustable up to 1000 V. The arc threshold was set to 120 A. If the current exceeded this value, the supply's arc suppression mechanism would be triggered, rapidly terminating the pulse-driving voltage. We used a pulse length of typically 400 μs. In the case of Ti and Nb and high applied voltage, we had to use shorter pulse lengths to protect the equipment.

Pure argon gas was supplied near the target, establishing an operational pressure that was adjusted by the specific combination of gas flow rate [up to 100 SCCM (SCCM denotes cubic centimeter per minute at STP)] and pumping speed (cryogenic pump and adjustable valve). At fully opened valve, the pumping speed was 1500 l/s for air, and the chamber base pressure was about 10^{-4} Pa. The total pressure was monitored by an MKS Baratron® gauge.

The discharge current was monitored using a current transformer (Pearson™ model 301X, 0.01 V/A, 2 MHz bandwidth), and the voltage at the target was measured with a 1000:1 voltage divider (Tektronix 6015A, 75 MHz bandwidth). The data were recorded on a digital storage oscilloscope (Tektronix TDS5104B) in sample mode.

The ion flux was measured using a differentially pumped mass and energy analyzer (EQP 300 by HIDEN Ltd.); the entrance aperture was at ground potential with an orifice of 100 μm diameter. The target-orifice distance was 10 cm. The total ion current was recorded using an ion collector of about 100 cm^2 area placed at 20 cm distance from the target; the collector was biased to −50 V with respect to ground.

The target materials were selected for their relevance in a number of applications as well as to investigate a diverse set of materials that would allow us to derive material-specific conclusions.

III. RESULTS

A. Copper

Copper was selected as a material of primary interest because of its relevance for semiconductor metallization and because it has one of the highest sputter yields of all metals (only exceeded by silver). The results for copper at different constant target voltages are compiled in Fig. 1. As the pulsed voltage exceeds 500 V, one can clearly see the development of an initial current peak of several amperes. Many other HIPIMS systems use relatively short pulses of typically only 10–50 μs, and therefore this initial peak is seen as *the* main feature.

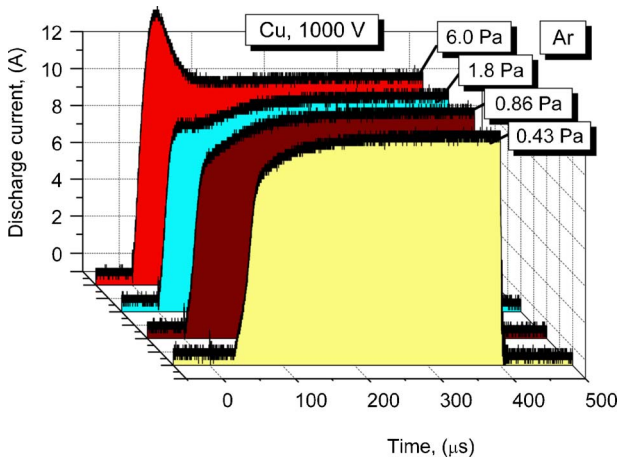

FIG. 2. (Color online) Current pulse shapes for different argon gas pressures when using a copper target. Note the pressure dependence of the initial peak but the relative independence later in the pulse.

The character of the ion current shape changes drastically when the applied "driving" voltage is increased by just an astonishingly small amount, in the example of Fig. 1 from 530 to 535 V. The current is not reduced anymore, as it was at relatively low voltage, but rather a new process compensates the current reduction. The narrow voltage interval where the change is observed is well reproducible. This was checked by setting the voltage higher and lower than about 535 V several times.

Given the overwhelming evidence of research on HIPIMS by optical and mass spectroscopy,[12–15] this process can be associated with the appearance of large amounts of copper neutrals and ions, displacing argon. At voltages of 530 V and higher, the sputtered metal starts to greatly affect the discharge, and the current jumps because the feedback loop, as described by Eq. (1), appears to have reached the unity threshold.

Another argument for this interpretation is the pulse shape obtained at different argon gas pressures. Figure 2 shows that the initial peak increases with argon pressure whereas the current level later in the pulse is practically independent on the initial gas pressure. Figure 3 shows an enlarged view of the curve for 0.44 Pa, which later will be discussed in greater detail.

Of great interest is the flux of ions that actually arrives at the substrate. Figure 4 indicates that while the metal phase started to be important at 535 V (Fig. 1), we observe a large increase in ion flow only at higher discharge voltages (and related higher currents). The ion current collected at 20 cm distance from the target is very small at low driving voltage; it shows a remarkable increase after the discharge becomes dominated by metal, and it becomes disproportionately greater at higher driving voltages.

B. Titanium

Based on the sputter yields of Ti and Cu (Fig. 5), one would expect that less titanium atoms are supplied to the discharge plasma, and that titanium would exhibit the strong metal plasma character at higher power or later times compared to copper. As shown in Fig. 6, this was not the case. At

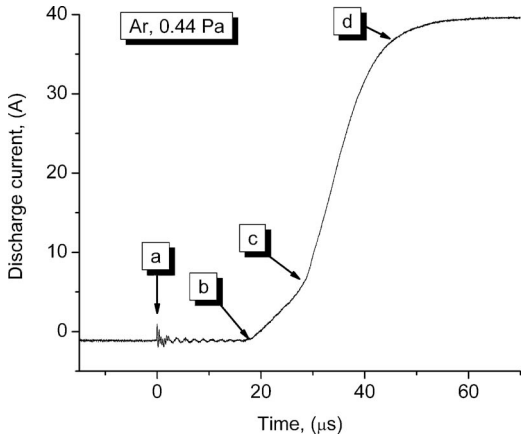

FIG. 3. Discharge current on copper target for an initial argon pressure of 0.44 Pa (corresponds to first curve shown in Fig. 2): Label *a* indicates the moment when the voltage is applied, *b* when the discharge starts, *c* when there is a change in the slope of the discharge current, and *d* when the current goes into saturation. The significance of these events is discussed in the text.

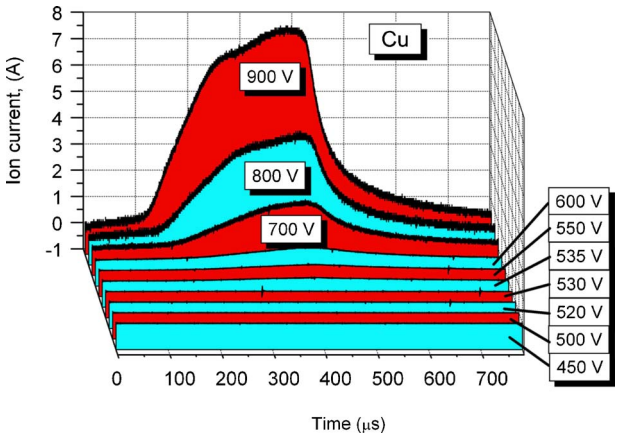

FIG. 4. (Color online) Ion current to an ion collector for HIPIMS copper discharges as a function of time, with the applied voltage as the parameter. The curves correspond to current pulses shown in Fig. 1.

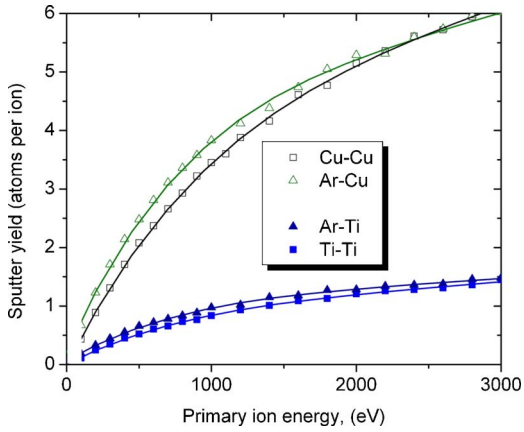

FIG. 5. (Color online) SRIM-calculated sputtering yields for primary argon ion and self-ion impact. Note that the high primary energies displayed here could be realistically obtained by multiply charged ions at high target voltage.

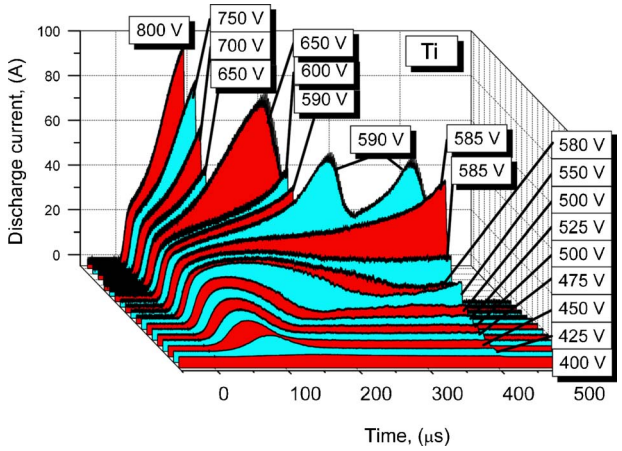

FIG. 6. (Color online) Current pulse shapes at different constant voltages for Ti discharges in argon at 1.8 Pa. The pulse length for higher driving voltage was precautionary reduced to not damage power supply and magnetron. Note that each curve is taken from a single pulse. In the transitional region around 585 V, several examples are shown to illustrate the irregular pulse shapes observed right at this threshold to the self-sputtering-dominated mode.

low voltage, the current shapes for the Cu and Ti targets are similar, namely, they show a peak at about 50 μs after the initial current rise. It is typical that the initial current rise is delayed by 50 μs or more with respect to the application of the voltage, which defines time equal to 0. The current amplitude with a titanium target is higher than with a copper target, which points to the importance of secondary electron emission and ionization caused by it.

In the transitional region at about 590 V, when the discharge current tends to be much higher after the initial peak, the current pulse form is not stable and reproducible. Instead, pulses may be either still of the low-current type or of the high current type, and in some cases, the current shape jumps in between these extremes. Each curve of Fig. 6 is a single pulse sample, and in the transitional region, more than one curve for a given voltage is shown to illustrate the great variations in the current-voltage-time space.

Figure 7 shows some measurements using the HIDEN energy and mass analyzer. The instrument's orifice was placed at 10 cm distance from the target, and the influx was integrated over 50 μs HIPIMS pulses. Despite the relatively short—by the standards of our investigation—pulse length, we can clearly see the appearance of titanium ions, including Ti^{2+}. Note that even doubly charged argon ions are detected. One can also see the rarefaction effect by the fact that the total ion count rate is reduced when the discharge current exceeded 10 A.

C. Niobium

Like titanium, the set of curves describing the current evolution for the niobium target indicates that high currents are reached readily albeit the onset of the high current occurs at even lower voltages (Fig. 8), which might be affected by the fact that this target was only 1/8 in. (3.1 mm) thick, and therefore the magnetic field on the target surface and on the sheath and presheath regions was higher. At about 500 V, the discharge jumps to a much higher current at the usual initial

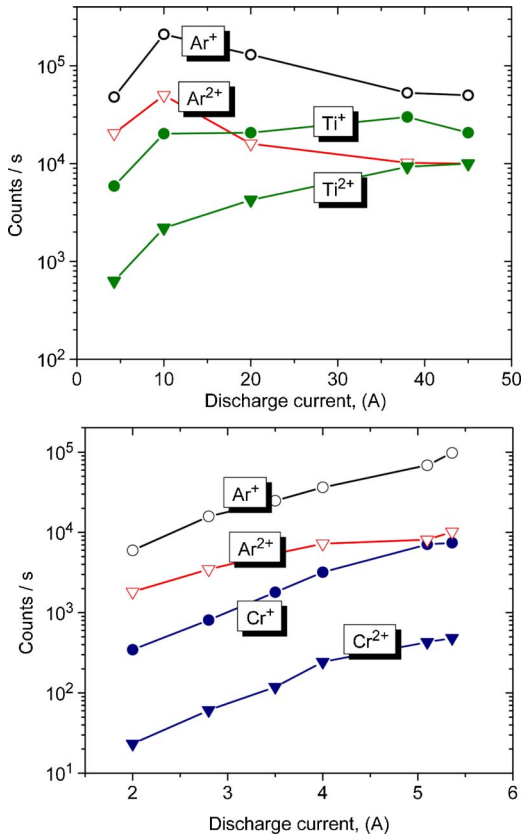

FIG. 7. (Color online) Ion flux integrated over 50 μs pulses as a function of the peak current (end of pulse) measured 10 cm from the target using the HIDEN EQP plasma analyzer for titanium (top) and chromium (bottom).

peak. In fact, when the voltage was set to 550 V, the current increase was so dramatic that the power supply's arc suppression interpreted the current rise as an arc, temporarily terminating the voltage. After a very short waiting period, the system applied the voltage again only to find that the current rises very fast. By the time the second pulse approached the current limit, the overall designated pulse length of 400 μs was reached. This behavior was reproducible. Given the current limitation of the power supply, it was not possible to go the higher voltages for the niobium target.

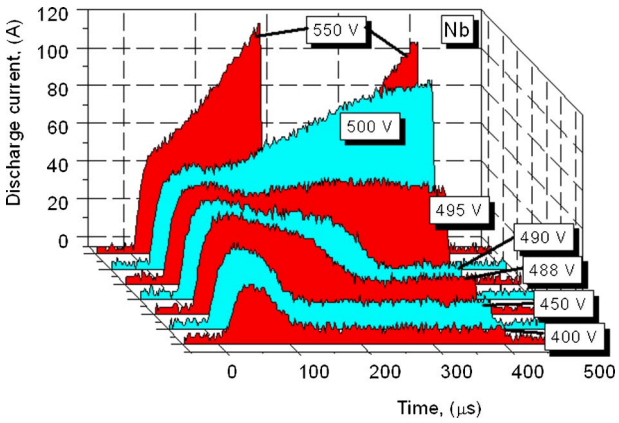

FIG. 8. (Color online) Current pulse shapes at different constant voltages for Nb discharges in argon at 1.8 Pa. The curve at 550 V was clipped by the arc suppression circuit (see explanation in text).

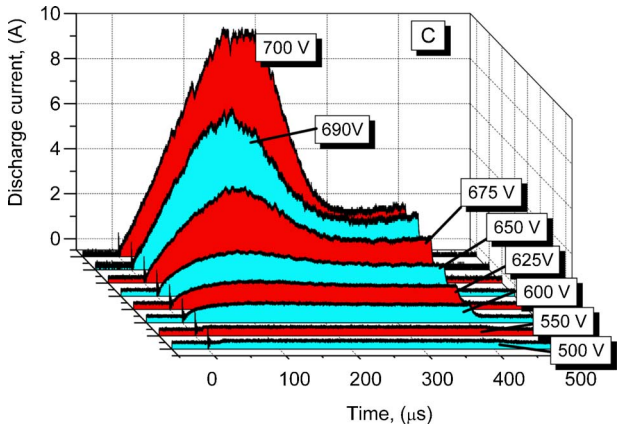

FIG. 9. (Color online) Current pulse shapes at different constant voltages for discharges with a graphite target in argon at 1.8 Pa.

D. Carbon (graphite)

The other extreme, compared to niobium, was the behavior of graphite (Fig. 9). Here, the current curves are essentially characterized by the initial peak each exhibits. At later times and higher voltages, one can see a slight increase in current but it remains at a relatively low level. Unfortunately, it was not possible to utilize the full voltage capability of the power supply because the discharge tended to arc when the voltage was set to 800 V or higher.

E. Tungsten

The tungsten discharge shows a significant current level after the initial peak when the applied voltage was 700 V or higher (Fig. 10). The most striking feature is the very steep increase of the initial peak, indicating that the argon gas is very efficiently ionized. The transitional phase, where the high current level starts to appear, is around 700 V, and the curves at about 720 V vary from pulse to pulse.

F. Aluminum

Aluminum generally shows a similar behavior, with the transition to a high level of current starting at about 550 V (Fig. 11). The current at later times exceed the initial peak

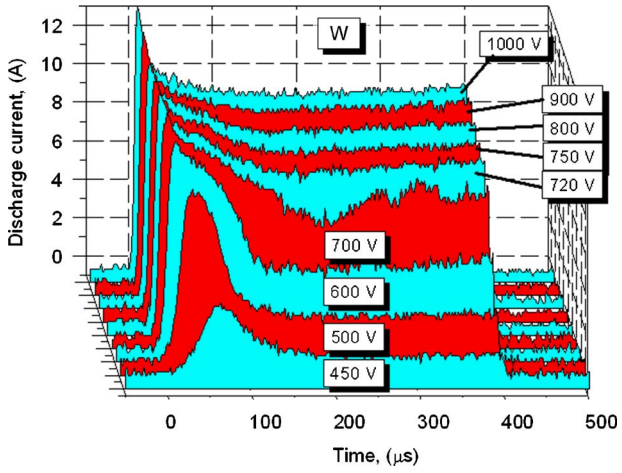

FIG. 10. (Color online) Current pulse shapes at different constant voltages for discharges with a W target in argon at 1.8 Pa.

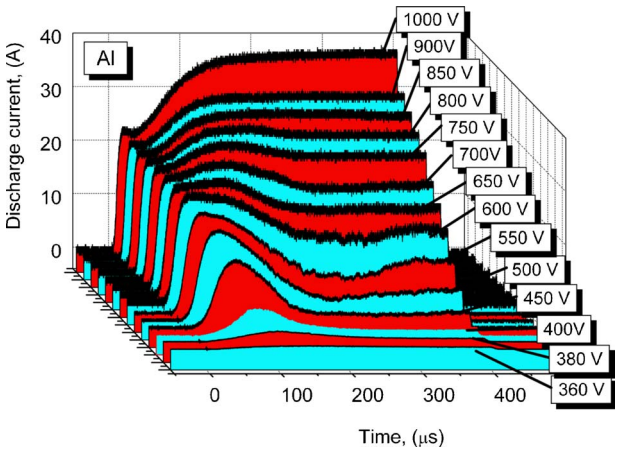

FIG. 11. (Color online) Current pulse shapes at different constant voltages for discharges with a Al target in argon at 1.8 Pa.

for voltages greater than about 700 V. As with copper, the aluminum discharge pulses are characterized by a new equilibrium, as indicated by the constant current later in the pulse.

G. Chromium

The chromium current was low, reaching maximum values of only 7 A at 1000 V, the maximum voltage of the power supply. This was surprising given the relatively high self-sputter yield of chromium. The curves showed a couple of interesting features (Fig. 12). The current after the initial peak increased steadily when the voltage was increased, whereas the initial peak showed some unusual minimum at about 550 V. This strange feature in the set of current curves was repeatedly reproduced by increasing and decreasing the voltage level. Measurements of the ion flux using the HIDEN EQP spectrometer indicated the presence of singly and doubly charged chromium and argon ions (Fig. 7, bottom).

IV. DISCUSSION

A. Some basic physics of the HIPIMS discharge

In the following discussion, we start with describing some general processes of the HIPIMS discharge, followed by a more specific discussion of the results described in Sec. III.

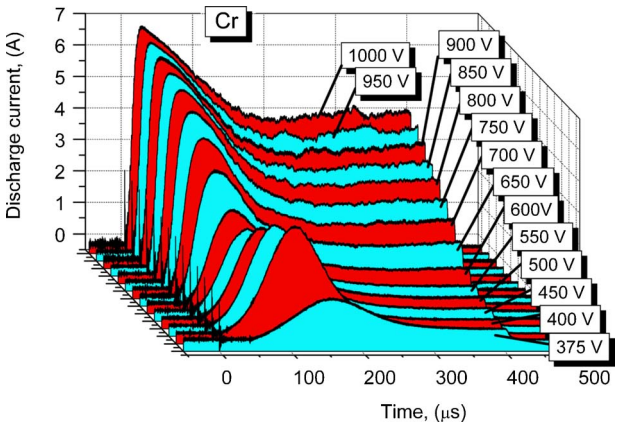

FIG. 12. (Color online) Current pulse shapes at different constant voltages for discharges with a Cr target in argon at 1.8 Pa.

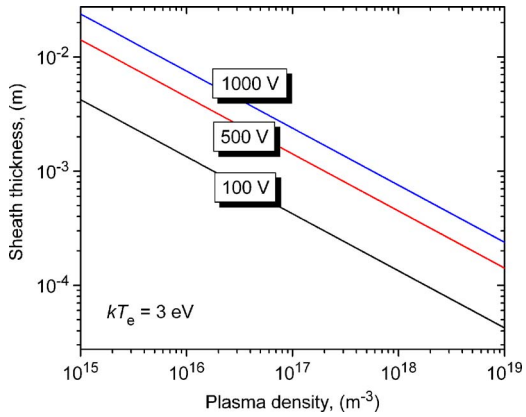

FIG. 13. (Color online) Child sheath thickness as a function of plasma density, with electron temperature and sheath voltage as parameters.

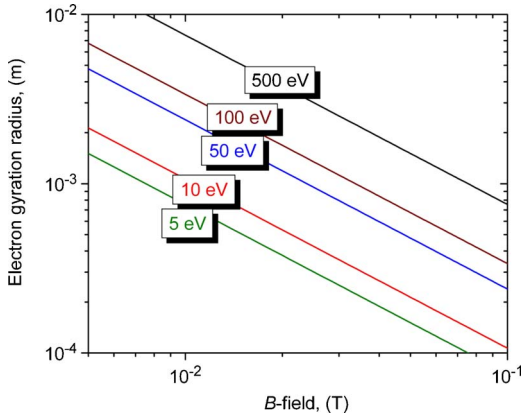

FIG. 14. (Color online) Gyration radius for electrons as a function of magnetic induction, with the energy-equivalent voltage as a parameter.

To describe the pulsed discharge, we initially neglect the contribution of the magnetic field for the sake of simplicity. Of course, the magnetic field plays a very important role, especially for the closed-drift motion of electrons, the probability of generating ions by impact ionization, and the ambipolar diffusion of plasma particles toward the substrate. We will include these effects later in the discussion.

As a negative voltage pulse is applied to the target, the development of the sheath depends strongly whether or not plasma is present. If none is there, plasma and sheath will form with some delay via mechanisms that include electron-gas interaction and Townsend avalanches. If plasma is already present when the voltage is applied, the initially very thin sheath responds with a characteristic time of the inverse electron plasma frequency, which is generally in the submicrosecond regime.[16] Therefore, electron response and sheath development are determined by the pulse rise time rather than electron inertia. The sheath expands further as the (argon) ions are accelerated toward the target surface; the sheath thickness asymptotically approaches a new equilibrium value. If we take the Child law, which can be applied to determine the thickness of a collisionless sheath,[17,18] we have

$$s(t) = \frac{3}{4}\left[\frac{\varepsilon_0^2 V_{\text{sheath}}^3(t)}{e n_0^2(t) k T_e(t)}\right]^{1/4}, \tag{2}$$

where ε_0 is the permittivity of free space, e is the elementary charge, k is the Boltzmann constant, V_{sheath} is the voltage drop in the sheath, n_0 is the plasma density, and T_e is the temperature of plasma electrons. Figure 13 shows the Child sheath width for relevant voltage and plasma parameters. The sheath is dynamic such that it is greatly dependent on the sheath voltage and plasma density at the sheath edge, and to a lesser degree, on the electron temperature.

The sheath evolution is greatly affected by the prepulse plasma density near the target: in the case of widely spaced pulses and the absence of a "keeping" plasma, the rise of current is often substantially delayed with respect to the applied voltage due to a statistical time lag for electrons to develop ionization avalanches and finally plasma (the delay exhibits a surprisingly high pulse-to-pulse reproducibility). The example shown in the original paper of Kouznetsov *et al.*[11] is typical for this situation.

A low-power keeping discharge or operation at high duty cycles ensures that the applied HIPIMS pulse can immediately lead to a strong rise in discharge current because there are enough ions near the target available to be accelerated. In contrast to conventional plasma immersion ion implantation models,[19] the plasma density is strongly dependent on the fluxes of secondary electrons and sputtered atoms coming from the target. The sheath thickness is a complicated issue because the plasma evolves, too, and not just the sheath, and the magnetic field is changing the electron dynamics and thereby indirectly the ion dynamics.

Ions impacting the target surface cause two main secondary processes: (i) emission of secondary electrons and (ii) sputtering of atoms. Both processes deserve deeper considerations.

Secondary electrons (SEs) are crucial for maintaining the discharge because the secondary electrons gain energy by traveling through the electric field of the sheath; they can directly cause ionization via impact ionization or indirectly via heating of the less energetic electrons in the bulk of the energy distribution function (plasma electrons).

The trajectory of a SE is curved due to the magnetic field of the magnetron. Gyration starts immediately when the electron is leaving the target surface. Using z as the coordinate normal to the target surface, the electron gyration radius is

$$r(z) = \frac{m_e v_\perp(z)}{eB} = \sqrt{\frac{2V_e(z)m_e}{eB^2}}, \tag{3}$$

where m_e is the electron mass, $v_\perp(z)$ is the velocity perpendicular to the direction of the magnetic field, V_e is the corresponding energy (in volts), and B is the magnetic induction. As the electron moves in the electric field of the sheath, it will be accelerated and picks up energy in the first part of its cyclic gyration motion; the exact amount depends on the potential difference between target surface and the most distant point of the trajectory from surface (Fig. 14).

SEs emitted in the center of the racetrack, where the magnetic field is perfectly parallel to the surface, will complete only one-half period of a cycloidal motion and return to the target surface—they do not contribute to the discharge unless they experience a collision or transfer energy via collective processes.

SEs emitted outside the very center of the racetrack can permanently escape from the target because of the tilt of the magnetic field relative to the surface. Those SE will periodically gain and lose energy as the gyration occurs. Their trajectory is cycloidal leading to the well known drift motion that is perpendicular to both the electric and magnetic field vectors ($\mathbf{E}\times\mathbf{B}$ drift[20]). The curved shape of the magnetic field brings drifting electrons back to their original position (provided no collisions occurred) and one obtains the closed-drift Hall current. One should note that this drift applies to the electrons only because the ions are too massive to be "magnetized," i.e., their gyration radius [Eq. (3)] by far exceeds the sheath and presheath size.

If one compares the Child sheath thickness (Fig. 13) and the gyration radius (Fig. 14), one can see that both are comparable. In fact, a SE leaves the surface with just a few eV and picks up energy, but for small magnetic field vectors tilts, it may stay in the sheath for some time. This has interesting implications, namely, that (i) the positive space charge in the sheath is "diluted" by electrons, and therefore the actual sheath thickness is larger than the Child sheath approximation, and (ii) collisions will occur inside the sheath, leading to the generation of ions and more electrons.

SEs emitted far from the racetrack center will experience a significantly tilted magnetic field which allows them to readily leave the sheath and to become energetic electrons (up to the full sheath voltage). They oscillate in the presheath plasma, each time reflected back into the presheath plasma when they reach the sheath edge. Of course, since there is an appreciable electric field in the presheath, they also participate in the $\mathbf{E}\times\mathbf{B}$ drift, though at a much smaller drift velocity than the electrons that are still in the sheath. Whether trapped in the sheath or oscillating in the presheath plasma, each SE will contribute to the generation of many ion-electron pairs.

If an ion is formed within the sheath or presheath, it will be accelerated toward the target surface by the electric field (the return probability β is close to unity) and it may cause further secondary electron emission and sputtering. The yields for these processes depend on the kinetic and potential energies of the ion (projectile). While the sputter yields can be readily calculated using for example the TRIM or SRIM codes,[21] the yield of secondary electrons is a much more complicated issue. Generally, one distinguishes between kinetic and potential electron emissions. Much work has been done by Winter *et al.*[22,23] and others,[24,25] and here we summarize their results in a very simplified manner. Kinetic emission (KE) is dominant at about >300 eV/amu projectile energies (where "amu" stands for the atomic mass number of the projectile ion), i.e., much greater than the typical kinetic energies observed and expected in a HIPIMS discharge. KE is subject to a classical threshold but emission is still observed down to the "apparent" threshold, which is all the way down to the ~10 eV/amu region. However, the KE yield is then 10^{-3} or smaller and therefore negligible. For the relevant low kinetic energies of HIPIMS ions, we need to consider the emission determined by the *potential* energy of the arriving ion projectile [potential emission (PE)].

TABLE I. Work function ϕ and first and second ionization energies for selected materials.

	ϕ (eV)	$E_{0\to1}$ (eV)	$E_{1\to2}$ (eV)
Ar	N/A	15.76	27.63
Cu	4.9	7.73	20.29
Ti	4.1–4.3	6.82	13.58
Nb	3.96	6.88	14.32
C	4.53	11.26	24.38
W	4.55	7.98	17.62
Al	4.08–4.28	5.99	18.83
Cr	4.5	6.77	16.50

PE requires that the potential (ionization) energy of the arriving ions exceeds twice the work function of the material ϕ. Experimental data of the yields for various ions satisfy the fit[24]

$$\gamma_{\mathrm{PSEE}} = 0.032(0.78E_i - 2\phi). \tag{4}$$

The factor 2 arises from the fact that one electron is needed to neutralize the arriving ion and the second is the one that is emitted. As we can see from Table I, singly charged metal ions do not satisfy the condition

$$0.78E_i > 2\phi, \tag{5}$$

as required by Eq. (4) in order to obtain any PE. Hence, for a typical magnetron discharge, singly charged metal ions cause neither KE nor PE. In contrast, Ar^+ ions can cause PE due to its high ionization energy. We will return to this point in Sec. IV B when discussing specific results.

Much has been written about sputtering[26–28] and ionized sputtering.[1,15,29] For the latter, a key issue is to use process parameters and a suitable geometry such that the probability of ionization is high for the sputtered atoms before they reach the substrate. This is generally achieved by increasing the background gas pressure, making it likely that the sputtered atoms collide with gas, thereby slowing them down for a longer residence time in the plasma.

Using z as the coordinate normal to the target surface, the flux of sputtered atoms from the surface is reduced by[30]

$$d\Gamma_a = -\sigma_{ag}\Gamma_a n_g dz, \tag{6}$$

where σ_{ag} is the cross section for atom-gas collision and n_g is the gas density, with

$$n_g = p/kT_g, \tag{7}$$

where p is the pressure and T_g the gas temperature. If σ_{ag} is independent of position, one obtains

$$\Gamma_a(z) = \Gamma_a(0)\exp(-z/\lambda_{ag}), \tag{8}$$

with the mean free path

$$\lambda_{ag} = \frac{1}{n_g\sigma_{ag}} = \frac{kT_g}{p\sigma_{ag}}, \tag{9}$$

where we used the ideal gas equation [Eq. (7)]. The cross section σ_{ag} is not precisely known for all the atom-gas combinations, but it is generally in the range of $(10-40)\times10^{-20}$ m^2, with the lower values at higher kinetic energy of the colliding particles. Equation (9) includes the rarefaction

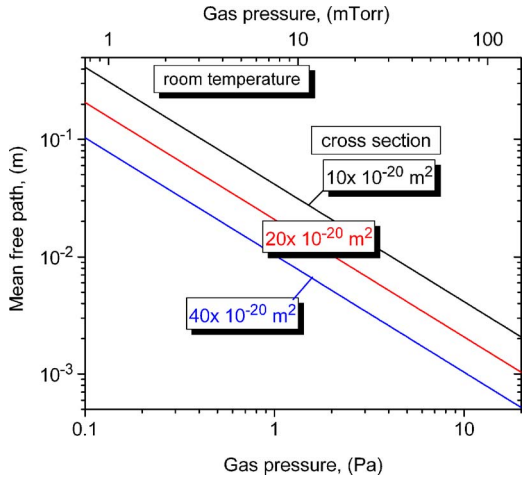

FIG. 15. (Color online) Parametric presentation of the mean free path for fast atoms in gas; the mean free path increases proportionally with the gas temperature.

effect, namely, as the local temperature increases during operation, the local gas density decreases and the mean free path increases proportionally. Figure 15 shows the mean free path assuming the gas at room temperature.

At a typical pressure of, say, 1 Pa (7.5 mTorr), the mean free path of atoms is larger than the sheath thickness, and only a small fraction $f \approx s/\lambda_{ag}$ of sputtered atoms will be slowed by a collision in the sheath. The important effect of collisions, apart from increasing the chance of ionization, is the feedback that slowed sputtered atoms can provide: they themselves can become part of the "gas" that can slow down sputtered atoms. That means that the gas density n_g in Eq. (6) is a highly dynamic variable, depending on both heating (rarefaction) and generation of sputtered, slowed atoms. Clearly, these processes evolve during the pulse duration, and therefore the experiments were done with relatively long pulses, allowing us to detect material dependent features.

B. Interpretation of the material and time dependent current-voltage characteristics

The current at the target is generally composed of the ion current and secondary electron current,

$$I(t) = [1 + \gamma_{\mathrm{SE}}(E_{\mathrm{pot}})]I_i(t), \tag{10}$$

where γ_{SE} is the secondary electron yield, which depends mainly on the potential energy of the arriving ions. The motion of ions is not very much affected by the presence of the magnetic field, and therefore one may approximate the ion current by the Bohm current,[31]

$$I_i = \int (0.61\bar{Q}en_0 v_{\mathrm{Bohm}})dA, \tag{11}$$

where $\bar{Q}$ is the average charge state number, with the ion sound velocity (Bohm velocity)

$$v_{\mathrm{Bohm}} = \sqrt{kT_e/m_i}. \tag{12}$$

The integration in Eq. (11) is over the target area. A typical feature of the current curves at low and moderate voltage (or, equivalently, power) is the appearance of the initial current peak, which can be ascribed to gas ion current and rarefaction due to gas heating.[32] In a pulsed system such as the HIPIMS system, we should expect strong pressure transients in front of the target;[33] however, the processing chamber acts like a large "pressure reservoir," thereby making the overall heating quasi-isobaric, i.e., after a spike the pressure returns to the chamber pressure. If we use the ideal gas equation [Eq. (7)] and Dalton's law,

$$p = \sum_{\alpha} n_\alpha kT_\alpha, \tag{13}$$

where the summation is over all kinds of particles α, we see that heating implies a reduction of the heavy particle (atom, ion) density, followed by a reduction of the ion flux to the target [see Eq. (11)]. Additionally, one should expect that the pressure is not isotropic, as implied in Eq. (13), but that the "wind" of sputtered atoms displaces argon atoms preferentially in a direction normal to the target surface.

The sputter yields are mainly determined by the surface binding energy of the target material, and to a lesser degree, by the kind of ions arriving at the target. Figure 5 shows examples of sputter yields for primary argon ion and self-ion impact as calculated by the SRIM MONTE CARLO code.[21] The high primary energies displayed here could be realistically obtained by multiply charged ions at high target voltage. As the HIPIMS pulse progresses, argon ions are partially replaced by metal ions. The degree and speed of this replacement depend on the target material, gas pressure, and on the applied voltage. Gas ion replacement may reach a threshold such that the condition of sustained self-sputtering [Eq. (1)] is satisfied: the system will switch into a qualitatively and quantitatively very different mode, characterized by a higher current. Higher current implies higher power, and indeed, one can see that the magnetron's optical emission jumps to higher brightness and it also changes color. This switching is very obvious for most materials. For example, for copper or niobium at an argon pressure of 1.8 Pa, the brightness jumps when the voltage is increased from 530 to 535 V (Fig. 1) and from 490 to 500 V (Fig. 8), respectively. The color change is related to the change of excitations conditions and type and density of excited species. Detailed spectroscopic investigations will provide greater insight.

If the power setting is high, for example, if we consider the case of copper with an applied voltage of 800 V, i.e., a voltage clearly higher than the threshold of 535 V, the transition to the self-sputter-dominated mode occurs within the initial current peak (Fig. 2). At low pressure, one can discern this onset by a change of the slope of the current curve (moment *c* in Fig. 3).

While self-sputtering is associated with a feedback mechanism that leads to amplification of sputtering and ionization, there is also an increase in "losses" of sputtered atoms from the target zone. These losses eventually start to compensate the generation processes (time *d* in Fig. 3); the flat curve after time *d* indicates that the discharge has found a new steady state. Losses to the magnetron processes imply that the flux of sputtered material becomes available in areas remote to the target (e.g., the substrate) and contribute to the

deposition rate. The steady state is reached faster when the applied voltage is higher because all processes are driven at greater rates.

There are several interesting features in the ion current curves of Fig. 4. After about the first 100 μs, the slope of the curves is suddenly steepening, which seems to coincide with the time when metal overtakes rarefaction of argon. This is most pronounced at high voltage (or power). One can also see that the ion current at 20 cm distance tends to increase throughout the pulse even as the discharge parameters have found new steady-state values. This cannot be attributed to the drift processes from the target to the more distant location of the collector because the delay time between discharge termination and the start of ion current decay is about only 20 μs, i.e., the information of pulse termination was transported to the ion collector with about 10^4 m/s. The ion current rise and fall times are much longer, which is indicative for the importance of metal plasma evolution and collisional processes.

The ion flux pattern can be affected by the magnetic field of the circular $\mathbf{E}\times\mathbf{B}$ drift current (Hall current), especially when the discharge current is high (>50 A). The Hall current is in a doughnut-shaped zone just above the "racetrack;" it can exceed the discharge current by about a factor of 3.7 (dc magnetron with copper target and argon gas[34]) or somewhat less for pulsed systems.[35,36] While plasma confinement near the racetrack remains largely unaffected, the field of the Hall current may alter the weak field region far from the target and may facilitate increased ion flow to the substrate, as shown in Fig. 4 for copper.

The results for the other target materials show qualitatively similar features. However, it was surprising to find that the level of target current at the onset of the self-sputter-dominated phase did not correlate with the self-sputter yield. It shows again that the condition $\gamma_{SS}>1$ is a necessary but not the sufficient condition, and that secondary electron emission yield, magnetic confinement of secondary electrons, and their ability to ionize the target atoms are critical to reaching the self-sputter-dominated mode. These factors are very different for the various target materials. Here we point out a few features.

After onset of the self-sputter mode, the current for Ti and Nb did not reach steady state for the discharge conditions of our experiment: the feedback processes and current amplification of self-sputtering led to rising currents exceeding the limit of the power supply. The ionization of Ti and Nb atoms seems to occur very efficiently. One factor is the high yield of secondary electrons, which can be attributed to a relatively low work function (Table I). One may speculate that these reactive transition metals may have formed dielectric layers that additionally enhance the yield.

Another possible factor is that the ionization energy to obtain doubly charged ions is relatively low; hence, the concentration of doubly charged ions is expected to be high. This point is important because it will critically affect the secondary electron yield. As mentioned earlier, singly charged metal ions do not cause PE and their kinetic energy is too low until it exceeds the apparent threshold of about 10 eV/amu (this has been nicely demonstrated for the case of gold[37]). Therefore, we suggest that *multiply* charged metal ions play a critical role for the onset and maintenance of the self-sputter-dominated phase. If one generalizes condition (5) to multiply charged ions, there should be a consideration of the ion's total ionization energy on the one hand, and the total work function of all emitted electrons, at least $(Q+1)\phi$, on the other hand, where Q is the charge state number of the arriving ion (Q electrons are needed for neutralization, and at least one is actually emitted). Generally,

$$\sum_{Q'}^{Q} E_{Q'\to Q'+1} > (Q+1)\phi \tag{14}$$

is satisfied by a wide margin by metal ions with charge state $Q>1$. The presence of multiply charged ions in HIPIMS discharges has been detected by optical emission spectroscopy[12,13] and by particle spectroscopy. For example, Fig. 7 shows measurements of Ti and Cr, where not only doubly charged metal ions are detected but also doubly charged argon, whose ionization energy is even higher (Table I).

We conclude the discussion by looking at the other materials. Carbon (graphite target) is a semimetal. It is a special case because carbon has a very small sputter yield (Fig. 16). Condition (1) can therefore never be satisfied, i.e., carbon does not go in the self-sputter dominated mode. The current level after the initial peak does not reach the high level seen with other target materials. Carbon is also special because it has a low mass (higher atom velocity) as well as higher ionization energy than the true metal targets. This means that sputtered carbon atoms are less likely to become ionized. However, once ionized, the *singly* charged ion can cause PE [see condition (5)]. Due to the lower ionization, the atom's low mass, and the low flux of sputtered atoms, the rarefaction of argon is much slower: the initial peak is much wider than with other target materials.

The situation for tungsten is in great contrast to carbon (Fig. 10). Tungsten is easily ionized, its atomic mass is greater than the argon mass, which is important for the collisions leading to argon rarefaction, and the escape velocity of sputtered atoms slow. The rise time of the initial current

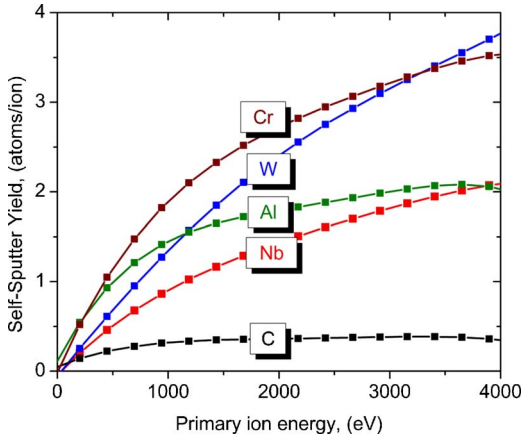

FIG. 16. (Color online) Self-sputter yields for various target materials as a function of primary ion kinetic energy, as calculated by SRIM code. For copper and titanium, see Fig. 5.

peak is therefore very short, and the peak has a very small full width at half maximum. The transition to the self-sputter-dominated mode is observed at about 700 V of applied voltage, although the absolute current value does not reach or exceed the initial (argon ion) peak value. The current signal for tungsten was noisier than for other materials, and in fact, some minor smoothing of the signal was necessary to keep the presentation of the curve set neat. This is in contrast to copper (Fig. 1) where the signal was very smooth. Since the current signal is dominated by ions arriving at the target, the noisiness reflects fluctuations in ion generation and possibly ion charge states. Based on the lower ionization energies and the presence of multiple charge states for tungsten on the one hand and many more "smoothing" charge exchange collisions for copper on the other hand, it is reasonable to expect greater fluctuations for tungsten.

Aluminum showed all of the previously mentioned effects (Fig. 11) but not in any extreme way. The transition to the self-sputtering-dominated mode occurred at an applied voltage of about 600 V but here in a more gradual manner. Aluminum and some other materials showed low-frequency instabilities under certain conditions—we will report on those effects in a separate publication.

Chromium showed a surprisingly low current (Fig. 12). The metal-dominated mode does not seem to be established within the parameter range investigated—there is at best a mode in which both argon and metal ions play a role. Based on experiments with chromium using another higher voltage system at the Sheffield Hallam University, we believe we would have reached the metal-dominated phase in this experiment if the voltage was greater than 1 kV. However, we do not have a convincing explanation for the minimum of the initial (argon ion) peak observed at a voltage of 550 V, and for the differences to other metals such as tungsten, for example, given that work function, ionization energies, and sputter yields are not very different.

V. SUMMARY AND CONCLUSIONS

High power impulse magnetron sputtering (HIPIMS) discharges are characterized by a peak power density at the target exceeding conventional power densities by about two orders of magnitude or more. For orientation, the power density in the racetrack zone may reach a peak of 10 kW/cm^2, as opposed to the more conventional 100 W/cm^2 or less. Consequently, the plasma density is much higher and the sputtered atoms may become ionized.

The current study shows that the current-voltage-time characteristics strongly depend on the material but do not simply correlate with the self-sputter yields. This pointed to the important role of secondary electrons, their confinement by the magnetic field, and their ability to efficiently ionize sputtered atoms which will return to the target due to the presence of the electric field in the sheath and presheath. The yield of secondary electrons depends strongly on the potential energy of the primary ions, and therefore, we have reason to believe that the generation of multiply charged metal ions is critical for the onset and maintenance of the self-sputter-dominated phase.

The characteristics taken for constant voltage typically show an initial current peak, which can be ascribed to argon ions and secondary electrons generated by them, followed by a second phase which can be associated with sustained self-sputtering provided the power level is high enough. This supports similar findings by Macák *et al.*[38] for TiAl targets. While copper settled into a new steady-state phase, the current of titanium and niobium did not reach such steady state within the current limits of the power supply. Carbon did not go into a second high-current, self-sputter-dominated phase, which is not a surprise given the low sputter yield and high ionization energy. Other materials show the self-sputter-dominated phase in a more or less pronounced manner, the details of which call for time-dependent modeling of the discharge taking into account at least two spatial dimensions.

ACKNOWLEDGMENTS

The authors thank Günter Mark, David Horwat, and Joe Wallig for technical help and Thomas Schenkel for helpful discussions. A.E. and J.A. acknowledge support from EPSRC Grant No. EP/D049202/1 and the Wenner-Gren Foundations, respectively. This work was supported by the Assistant Secretary for Energy Efficiency and Renewable Energy, Office of Building Technology, of the U.S. Department of Energy under Contract No. DE-AC02-05CH11231.

[1] A. P. Ehiasarian, J. G. Wen, and I. Petrov, J. Appl. Phys. **101**, 054301 (2007).
[2] A. P. Ehiasarian, W. D. Munz, L. Hultman, U. Helmersson, and I. Petrov, Surf. Coat. Technol. **163–164**, 267 (2003).
[3] J. S. Colligon, J. Vac. Sci. Technol. A **13**, 1649 (1995).
[4] O. R. Monteiro, Annu. Rev. Mater. Sci. **31**, 111 (2001).
[5] A. Anders, J. Phys. D **40**, 2272 (2007).
[6] N. Hosokawa, T. Tsukada, and T. Misumi, J. Vac. Sci. Technol. **14**, 143 (1977).
[7] N. Hosokawa, T. Tsukada, and H. Kitahara, Proceedings of the Eight International Vacuum Congress, Le Vide, Cannes, France, edited by F. Abeles, pp. 11–14 (1980).
[8] W. M. Posadowski, Thin Solid Films **392**, 201 (2001).
[9] W. M. Posadowski and Z. Radzimski, J. Vac. Sci. Technol. A **11**, 2980 (1993).
[10] S. P. Bugaev, N. N. Koval, N. S. Sochugov, and A. N. Zakharov, XVIIth International Symposium on Discharges and Electrical Insulation in Vacuum, Berkeley, CA, edited by S. Anders and A. Anders (LBNL, California, 1996), pp. 1074–1076.
[11] V. Kouznetsov, K. Macak, J. M. Schneider, U. Helmersson, and I. Petrov, Surf. Coat. Technol. **122**, 290 (1999).
[12] J. Vlček, P. Kudláček, K. Burcalová, and J. Musil, J. Vac. Sci. Technol. A **25**, 42 (2007).
[13] A. P. Ehiasarian, R. New, W.-D. Münz, L. Hultman, U. Helmersson, and V. Kouznetsov, Vacuum **65**, 147 (2002).
[14] J. Bohlmark, J. Alami, C. Christou, A. Ehiasarian, and U. Helmersson, J. Vac. Sci. Technol. A **23**, 18 (2005).
[15] U. Helmersson, M. Lattemann, J. Bohlmark, A. P. Ehiasarian, and J. T. Gudmundsson, Thin Solid Films **513**, 1 (2006).
[16] B. P. Wood, D. J. Rej, A. Anders, I. G. Brown, R. J. Faehl, S. M. Malik, and C. P. Munson, in *Handbook of Plasma Immersion Ion Implantation and Deposition*, edited by A. Anders (Wiley, New York, 2000), Chap. 4.
[17] A. T. Forrester, *Large Ion Beams* (Wiley, New York, 1988).
[18] A. Anders, Surf. Coat. Technol. **183**, 301 (2004).
[19] M. A. Lieberman, in *Handbook of Plasma Immersion Ion Implantation and Deposition*, edited by A. Anders (Wiley, New York, 2000).
[20] F. F. Chen, *Plasma Physics and Controlled Fusion* (Plenum, New York, 1984).
[21] J. F. Ziegler and J. Biersack, Monte Carlo code SRIM2006.02, 2006 (http://srim.org/).
[22] H. Winter, F. Aumayr, and G. Lakits, Nucl. Instrum. Methods Phys. Res.

B **58**, 301 (1991).
[23]H. Winter, H. Eder, F. Aumayr, J. Lorincik, and Z. Sroubek, Nucl. Instrum. Methods Phys. Res. B **182**, 15 (2001).
[24]R. A. Baragiola, E. V. Alonso, J. Ferron, and A. Oliva-Florio, Surf. Sci. **90**, 240 (1979).
[25]J. Lörinčík, Z. Šroubek, H. Eder, F. Aumayr, and H. Winter, Phys. Rev. B **62**, 16116 (2000).
[26]M. Kaminsky, *Atomic and Ionic Impact Phenomena on Metal Surfaces* (Springer-Verlag, Berlin, 1965).
[27]*Sputtering by Particle Bombardment I*, edited by R. Behrisch (Springer, Berlin, 1981).
[28]W. D. Westwood, *Sputter Deposition* (AVS, New York, 2003).
[29]*Ionized Physical Vapor Deposition*, edited by J. A. Hopwood (Academic, San Diego, CA, 2000).
[30]E. V. Barnat and T.-M. Lu, *Pulsed Sputtering and Pulsed Bias Sputtering* (Kluwer Academic, Boston, 2003).
[31]D. Bohm, in *The Characteristics of Electrical Discharges in Magnetic Fields*, edited by A. Guthrie and R. K. Wakerling (McGraw-Hill, New York, 1949), pp. 77–86.
[32]S. M. Rossnagel, J. Vac. Sci. Technol. A **6**, 19 (1988).
[33]K. B. Gylfason, J. Alami, U. Helmersson, and J. T. Gudmundsson, J. Phys. D **38**, 3417 (2005).
[34]S. M. Rossnagel and H. R. Kaufman, J. Vac. Sci. Technol. A **5**, 88 (1987).
[35]J. Bohlmark, U. Helmersson, M. VanZeeland, I. Axnas, J. Alami, and N. Brenning, Plasma Sources Sci. Technol. **13**, 654 (2004).
[36]A. Vetushka and J. W. Bradley, J. Phys. D **40**, 2037 (2007).
[37]H. Eder, W. Messerschmidt, H. Winter, and F. Aumayr, J. Appl. Phys. **87**, 8198 (2000).
[38]K. Macák, V. Kouznetsov, J. Schneider, U. Helmersson, and I. Petrov, J. Vac. Sci. Technol. A **18**, 1533 (2000).